

High spin expansion for null geodesics

Peng-Cheng Li^{1,2}, Minyong Guo^{1*}, and Bin Chen^{1,2,3}

¹*Center for High Energy Physics, Peking University, No.5 Yiheyuan Rd, Beijing 100871, P. R. China*

²*Department of Physics and State Key Laboratory of Nuclear Physics and Technology, Peking University, No.5 Yiheyuan Rd, Beijing 100871, P.R. China*

³*Collaborative Innovation Center of Quantum Matter, No.5 Yiheyuan Rd, Beijing 100871, P. R. China*

Abstract

We consider the high spin expansion for the null geodesics in the Kerr spacetime. We expand the null geodesic equation successively to higher orders in deviation from extremity. Via the method of matched asymptotic expansion, the radial integrals are obtained analytically. It turns out that the analytic expressions are very sensitive to the value of the shifted Carter constant q . We show that for a large q , the analytic expressions can be used to study observational electromagnetic signatures for astrophysical black holes like M87*. However, for a small q , the high spin expansion method can only be applied to (near-) extreme black holes.

Email: lipch2019@pku.edu.cn, minyongguo@pku.edu.cn, bchen01@pku.edu.cn

* Corresponding author.

1 Introduction

The Event Horizon Telescope (EHT) had enough participants to enable the array to reach sufficient angular resolution to image the supermassive black hole in Sagittarius A* and M87* for the first time in April 2017 [1]. From then on, a new page has been turned in astronomical black hole physics. Experimental data are constantly being obtained, which brings not only excitement but also challenges. In other words, physicists need not only to process data, but also to make theoretical predictions about what the EHT will see. In April 2019, the mystery of the image of M87* was firstly solved, which helps to test Einstein's general relativity and other gravity theories [2–7]. However, this is only the first step and the next is to increase the number of telescopes to take pictures of the black holes in more detail and from more angles. As a result, theoretical research also has to be further developed.

As we know, the basic theoretical aspect of dealing with the observational electromagnetic signatures is the study of null geodesics in the black hole spacetime. In general, the integrals of the null geodesic equations are hard to perform analytically. Nevertheless, for an (near-) extreme Kerr black hole, the authors in [8] found that the radial integrals of the equations for null geodesics which start in the near-horizon region to an observer in the region far from the black hole can be solved analytically to the leading order in ϵ which characterizes the deviation from extremity. The rationale behind the strategy is due to the emergence of the enhanced conformal symmetry of the near-horizon geometry for the (near-) extreme Kerr black hole [9, 10].¹ Recently, this enhanced symmetry helps to simplify the gravitational dynamics greatly in the near-horizon region, see for instance [13–23].

As a prototypical example, [12] analytically computed the observational appearance of a light emitter on the inner most stable orbit of a (near-) extreme Kerr black hole. Moreover, as pointed out in [12], their results are valid only when the deviation parameter $\epsilon = 0.01$, which corresponds to the spin $a = 0.9999995M$. However, to our knowledge, the spin of rapidly spinning black holes in our universe cannot be so large. Theoretically, the black holes with geometrically thin disk models are subjected to the well-known Thorne bound $a \leq 0.998M$ [24]. Concerning the observation of EHT, the target high spin black hole is M87*. Recent researches have shown that the upper bound of the spin of M87* is about 0.9 [25, 26]. In consequence, the approximate analytic results obtained by treating M87* as a (near-) extreme Kerr black hole may not be applicable anymore. A possible remedy to overcome this shortcoming is to perform the radial integrals of the null geodesic equations by taking into account of the corrections of higher orders in ϵ , such that the spin could take a value relevant to the realistic supermassive black holes like M87*.

The aim of this paper is to investigate the feasibility of obtaining analytic results via expanding the dynamic equations of a rapidly spinning black hole in ϵ to high orders, which is called the high spin expansion. Based on the work of [8, 12], we would like to perform the high spin expansion for the radial integrals of the null geodesics in the Kerr spacetime. We first expand the null geodesic equations in ϵ successively including the leading order(LO), the next-to-leading order(NLO), and

¹The radial integrals of null geodesics can also be obtained analytically by using the $1/D$ expansion method, no matter the black holes are rotational or not [11].

even up to NNNLO corrections. With this, via the method of matched asymptotic expansions (MAE) we find that the radial integrals of the null geodesic equations can be obtained analytically order by order. The reliability of the approximate analytical results is crucially dependent on the values of the shifted Carter constant q . When q is large, the results matches well with the numerical integrals for a relatively small spin, e.g. $a = 0.9$, which confirms the effectiveness of the high spin expansion. However, if q takes a small value the high spin expansion method would be not so effective and the relative error of the approximate results to the numerical integrals increases quickly as the spin lowers from extremity. The explicit demonstration of the applications of the high spin expansion method in this paper may provide some hints in solving other dynamical equations.

The rest of the paper is organized as follows. In Sec. 2, we discuss the basis of null geodesics and the high spin expansion in the Kerr spacetime. In Sec. 3, we focus on the radial integrals of the null geodesic equations in the $r - \theta$ motion. Next, we turn to the radial integrals in $r - \phi$ and $r - t$ motions in Sec. 4 and 5, respectively. We provide concluding remarks in Sec. 6.

2 Null geodesics and the high spin expansion in Kerr spacetime

In this section, we would like to start with a brief review of null geodesics in Kerr spacetime. Then we turn to discuss the basic idea behind exploring the higher corrections to the radial integrals along the null geodesics, in the virtue of the high spin expansion and matched asymptotic expansion (MAE) at some length. Actually, this program was first mentioned in [8, 12], where they stopped at the calculations at the leading order however. As a consequence, our investigated results to the higher orders can be seen as an extension along this line.

2.1 Null geodesics in Kerr spacetime

In terms of the Boyer-Lindquist coordinates we have the Kerr metric in this form

$$ds^2 = -\frac{\Delta}{\hat{\rho}^2}(d\hat{t} - a \sin^2 \theta d\hat{\phi})^2 + \frac{\sin^2 \theta}{\hat{\rho}^2}((\hat{r}^2 + a^2)d\hat{\phi} - a d\hat{t})^2 + \frac{\hat{\rho}^2}{\Delta}d\hat{r}^2 + \hat{\rho}^2 d\theta^2, \quad (2.1)$$

where

$$\Delta = \hat{r}^2 - 2M\hat{r} + a^2, \quad \hat{\rho}^2 = \hat{r}^2 + a^2 \cos^2 \theta. \quad (2.2)$$

This describes neutral rotating black holes of mass M and angular momentum $J = aM$. The 4-momentum of a massless particle living in the spacetime takes the general form

$$p^\mu = (\dot{t}, \dot{r}, \dot{\theta}, \dot{\phi}), \quad (2.3)$$

where the dot denotes the derivative with respect to the affine parameter. In general, the motion of a particle is governed by the Hamilton–Jacobi equation, and the null geodesic equations are completely integrable in Kerr spacetime because of four conserved quantities along the trajectory of each photon: the invariant mass $p^2 = 0$, the total energy $\hat{E} = -p_t$, the component of angular momentum parallel to the axis of symmetry $L = p_\phi$, and the Carter constant $\hat{Q} = p_\theta^2 - \cos^2 \theta (a^2 p_t^2 - p_\phi^2 \csc^2 \theta)$.

The existence of the four conserved quantities enables integration of the null geodesic equations into the form [28]

$$\int^{\hat{r}} \frac{d\hat{r}'}{\sqrt{\hat{R}}} = \int^{\theta} \frac{d\theta'}{\sqrt{\hat{\Theta}}}, \quad (2.4)$$

$$\hat{\phi} = \int^{\hat{r}} \frac{a\hat{E}\hat{r}'^2 + (\hat{L} - a\hat{E})(\Delta - a^2)}{\hat{\Delta}\sqrt{\hat{R}}} d\hat{r}' + \int^{\theta} \frac{\hat{L} \cot^2 \theta'}{\sqrt{\hat{\Theta}}} d\theta', \quad (2.5)$$

$$\hat{t} = \int^{\hat{r}} \frac{\hat{E}\hat{r}'^2(\hat{r}'^2 + a^2) + a(\hat{L} - a\hat{E})(\Delta - \hat{r}'^2 - a^2)}{\hat{\Delta}\sqrt{\hat{R}}} d\hat{r}' + \int^{\theta} \frac{a^2\hat{E} \cos^2 \theta'}{\sqrt{\hat{\Theta}}} d\theta', \quad (2.6)$$

where

$$\hat{R} = (\hat{E}(\hat{r}'^2 + a^2) - \hat{L}a)^2 - \Delta(\hat{Q} + (\hat{L} - a\hat{E})^2), \quad (2.7)$$

$$\hat{\Theta} = \hat{Q} - \cos^2 \theta' \left(\frac{\hat{L}^2}{\sin^2 \theta'} - a^2\hat{E}^2 \right). \quad (2.8)$$

The trajectory of the photon is independent of its energy, thus for convenience we introduce two rescaled quantities,

$$\hat{\lambda} = \frac{\hat{L}}{\hat{E}}, \quad \hat{q} = \frac{\sqrt{\hat{Q}}}{\hat{E}}. \quad (2.9)$$

Note that since $Q = p_\theta^2$ when $\theta = \pi/2$, any photon passing through the equatorial plane must have a nonnegative Carter constant, and hence a real \hat{q} . To avoid the case that when Q is negative then \hat{q} is imaginary, our strategy is to constrain the photon emitter on the equatorial plane.

2.2 The high spin expansion for Kerr spacetime

In this subsection, we move to the high spin expansion for the Kerr spacetime and discuss the method of MAE. Let's start to introduce a small parameter to represent the deviation of the black hole from being extremity,

$$\epsilon^3 = 1 - \frac{a^2}{M^2}. \quad (2.10)$$

In [12], it was shown that for a light emitter orbiting near a high spin black hole, such as on the innermost stable orbit (ISCO), $\hat{\lambda}$ is of the form

$$\hat{\lambda} = 2M + \mathcal{O}(\epsilon), \quad (2.11)$$

which is near the superradiant bound ². To characterize this feature, as in [8] we introduce

$$\hat{\lambda} = 2M(1 - \epsilon\lambda). \quad (2.12)$$

Moreover, following [12] we introduce the shifted Carter constant

$$q^2 = 3 - \frac{\hat{q}^2}{M^2}. \quad (2.13)$$

²The superradiant bound is given by $\hat{E} = \Omega_H \hat{L}$, so for a high spin black hole one finds $\hat{\lambda} = 2M(1 + \epsilon^{3/2} + \mathcal{O}(\epsilon^3))$.

It turns out that a positive q^2 guarantees a geodesic originating in the near region of the horizon can reach out to the far asymptotically flat region. The non-negativity of Θ restricts the constant q and λ by the inequality [27]

$$-q^2 + \left(\sqrt{1-\epsilon^3} + 2\lambda\epsilon - 2\right)^2 + 3 \geq 0, \quad (2.14)$$

which in the high spin expansion is given by

$$4 - q^2 - 4\lambda\epsilon + 4\lambda^2\epsilon^2 + \epsilon^3 + \mathcal{O}(\epsilon^4) \geq 0. \quad (2.15)$$

It is convenient to introduce the dimensionless Bardeen-Horowitz coordinates

$$t = \frac{\hat{t}}{2M}, \quad \phi = \hat{\phi} - \frac{\hat{t}}{2M}, \quad r = \frac{\hat{r} - M}{M}. \quad (2.16)$$

In terms of the coordinates (2.16), the geodesic equations become

$$\int_{r_n}^{r_f} \frac{dr'}{\sqrt{R}} = \int_{\theta_n}^{\theta_f} \frac{d\theta'}{\sqrt{\Theta}}, \quad (2.17)$$

$$\phi_f - \phi_n = -\frac{1}{2} \int_{r_n}^{r_f} \frac{\Phi}{(r^2 - \epsilon^3)\sqrt{R}} dr + \frac{1}{2} \int_{\theta_n}^{\theta_f} \frac{(\epsilon^3 - 1) \cos^2 \theta - 4(\lambda\epsilon - 1) \cot^2 \theta}{\sqrt{\Theta}} d\theta, \quad (2.18)$$

$$t_f - t_n = \frac{1}{2} \int_{r_n}^{r_f} \frac{T}{(r^2 - \epsilon^3)\sqrt{R}} dr + \frac{1}{2} \int_{\theta_n}^{\theta_f} \frac{(1 - \epsilon^3) \cos^2 \theta}{\sqrt{\Theta}} d\theta, \quad (2.19)$$

where

$$\begin{aligned} R &= \left((r+1)^2 + 2\sqrt{1-\epsilon^3}(\lambda\epsilon - 1) - \epsilon^3 + 1\right)^2 - (r^2 - \epsilon^3) \left(-q^2 + \left(\sqrt{1-\epsilon^3} + 2\lambda\epsilon - 2\right)^2 + 3\right), \\ \Theta &= 3 - q^2 + (1 - \epsilon^3) \cos^2 \theta - 4(\lambda\epsilon - 1)^2 \cot^2 \theta, \\ \Phi &= (r+1) \left(r^3 + 3r^2 - r(\epsilon^3 - 4\lambda\epsilon) + 4\lambda\epsilon \left(\sqrt{1-\epsilon^3} - 1\right) - 3\epsilon^3 - 8\sqrt{1-\epsilon^3} + 8\right), \\ T &= (r+1) \left(r^3 + 3r^2 - r(\epsilon^3 - 4) + 4\lambda\epsilon\sqrt{1-\epsilon^3} - 3\epsilon^3 - 4\sqrt{1-\epsilon^3} + 4\right). \end{aligned} \quad (2.20)$$

The above integrals are of elliptic type and could be treated numerically. In this paper we will see that the integrals can be expanded as power-series of the small ϵ and at each order of ϵ the integrals can be performed analytically. But at first, we note there is a subtlety here. We consider the radial integrals initiate from the near-horizon region, that is,

$$r_n \ll 1, \quad (2.21)$$

and the radial integrals terminate at far region, that is

$$r_f \gg \epsilon. \quad (2.22)$$

Then the expansion in ϵ works well for r whin the far region, but for $r \sim r_n$, may not be valid anymore. Because in the near-horizon region, r could be as small as $\sim \epsilon$ and even smaller, which

leads to the violation of the expansion in ϵ . As analysed in [12], to guarantee that the geodesics can get all the way to the far region, the starting points must lie in the NEHK region, that is $r \sim \epsilon$ and a even closer region to the horizon such as the near-NHEK region ($r \sim \epsilon^{3/2}$) is not allowed, as in this case the photon would run into the turning point. In this case one can introduce an intermediate scale ϵ^p with $0 < p < 1$, satisfying

$$\epsilon \ll \epsilon^p \ll 1, \quad (2.23)$$

to separate the integration regions. For the integral in the first region $r_n \leq r \leq \epsilon^p$ we make the change of variable

$$x = r/\epsilon, \quad (2.24)$$

and then in both regions the radial integrals can be appropriately expanded in ϵ .

The intermediate scale bears double features, one is that $\epsilon^p \ll 1$ so it is in the near-horizon region, but at the same time since $\epsilon^p \gg \epsilon$, it also lies in the far region. Therefore, via the method of matched asymptotic expansion (MAE) one can perform the radial integrals of the null geodesic equations in the high spin expansion. More specifically, one first performs the radial integral in the near-horizon region, $r_n \leq r \leq \epsilon^p$, and in the far region, $\epsilon^p \leq r \leq r_f$, respectively. The matching of the solutions in the overlap regions $r \sim \epsilon^p$ eliminate the dependence on p .

3 The radial integral for the $r - \theta$ motion

Based on the discussion in the previous section, next let's compute the radial integrals practically using the high spin expansion and the method of MAE. In this section, we focus on the radial integral

$$I^\theta = \int_{r_n}^{r_f} \frac{dr}{\sqrt{R(r)}}, \quad (3.1)$$

for the $r - \theta$ motion, which can be separated into

$$I^\theta = I_n^\theta + I_f^\theta, \quad (3.2)$$

with

$$I_n^\theta = \int_{r_n}^{\epsilon^p} \frac{dr}{\sqrt{R(r)}}, \quad I_f^\theta = \int_{\epsilon^p}^{r_f} \frac{dr}{\sqrt{R(r)}}. \quad (3.3)$$

Then both I_n^θ and I_f^θ can be expanded in a series of ϵ , that is,

$$I_{n,f}^\theta = I_{n,f}^{\theta(0)} + I_{n,f}^{\theta(1)}\epsilon + I_{n,f}^{\theta(2)}\epsilon^2 + \dots \quad (3.4)$$

For brevity, in the following we will use the notations for integral at each order of ϵ , that is,

$$I_n^{\theta(i)} = \mathcal{F}_n^{\theta(i)}(\epsilon^{p-1}) - \mathcal{F}_n^{\theta(i)}(x_n), \quad (3.5)$$

and

$$I_f^{\theta(i)} = \mathcal{F}_f^{\theta(i)}(r_f) - \mathcal{F}_f^{\theta(i)}(\epsilon^p), \quad (3.6)$$

where $i = 0, 1, 2, 3, \dots$ and $x_n = r_n/\epsilon$.

First of all, to the leading order of ϵ , one can easily find

$$I_n^{\theta(0)} = \int_{x_n}^{\epsilon^{p-1}} \frac{dx}{\sqrt{\mathcal{R}_n(x)}} = \mathcal{F}_n^{\theta(0)}(\epsilon^{p-1}) - \mathcal{F}_n^{\theta(0)}(x_n), \quad (3.7)$$

$$I_f^{\theta(0)} = \int_{\epsilon^p}^{r_f} \frac{dr}{\sqrt{\mathcal{R}_f(r)}} = \mathcal{F}_f^{\theta(0)}(r_f) - \mathcal{F}_f^{\theta(0)}(\epsilon^p), \quad (3.8)$$

with

$$\mathcal{F}_n^{\theta(0)}(x) = \frac{1}{q} \log \left(q\sqrt{\mathcal{R}_n(x)} + q^2x + 4\lambda \right), \quad (3.9)$$

and

$$\mathcal{F}_f^{\theta(0)}(r) = -\frac{1}{q} \log \frac{q\sqrt{\mathcal{R}_f(r)} + q^2r + 2r^2}{r^2}, \quad (3.10)$$

where we have introduced

$$\mathcal{R}_n(x) = q^2x^2 + 4\lambda(\lambda + 2x), \quad (3.11)$$

$$\mathcal{R}_f(r) = r^2(r^2 + 4r + q^2). \quad (3.12)$$

One can see that both the upper limit of the radial integral $I_n^{(0)}$, i.e. $\mathcal{F}_n^{\theta(0)}(\epsilon^{p-1})$, and the lower limit of $I_f^{\theta(0)}$, i.e. $\mathcal{F}_f^{\theta(0)}(\epsilon^p)$, depend on the specific value of p . But one can find that the asymptotic form of $\mathcal{F}_n^{\theta(0)}(\epsilon^{p-1}) - \mathcal{F}_f^{\theta(0)}(\epsilon^p)$ is independent of p , which is essentially the application of the MAE.

In detail, since $\epsilon^{p-1} \gg 1$, one can expand $\mathcal{F}_n^{\theta(0)}(\epsilon^{p-1})$ as

$$\mathcal{F}_n^{\theta(0)}(\epsilon^{p-1}) = \frac{\log(2q^2) - (1-p)\log\epsilon}{q} + \frac{4\lambda}{q^3}\epsilon^{1-p} + \frac{\lambda^2(q^2-12)}{q^5}\epsilon^{2(1-p)} + \mathcal{O}(\epsilon^{3(1-p)}), \quad (3.13)$$

and since $\epsilon^p \ll 1$, one can expand $\mathcal{F}_f^{\theta(0)}(\epsilon^p)$ as

$$\mathcal{F}_f^{\theta(0)}(\epsilon^p) = -\frac{\log(2q^2) - p\log\epsilon}{q} - \frac{2}{q^3}\epsilon^p - \frac{(q^2-12)}{4q^5}\epsilon^{2p} + \mathcal{O}(\epsilon^{3p}). \quad (3.14)$$

We can see that the leading order of $\mathcal{F}_n^{\theta(0)}(\epsilon^{p-1}) - \mathcal{F}_f^{\theta(0)}(\epsilon^p)$ is indeed independent of p , with the higher order terms can be canceled by leading order terms of the higher order \mathcal{F} functions. For example, the second term in $\mathcal{F}_n^{\theta(0)}(\epsilon^{p-1})$ can counteract the first term in $\mathcal{F}_f^{\theta(1)}(\epsilon^p)$. Then as shown in [12], one obtains

$$I^{\theta(0)} = -\frac{1}{q} \log \epsilon + \frac{1}{q} \log \frac{4q^4r_f^2}{(q\sqrt{\mathcal{R}_n(x_n)} + q^2x_n + 4\lambda)(q\sqrt{\mathcal{R}_f(r_f)} + q^2r_f + 2r_f^2)}. \quad (3.15)$$

The above procedure works straightforwardly when we proceed to the radial integrals expanded at higher orders in ϵ , i.e. $I^{\theta(i)}$ for $i \geq 2$. In order to obtain the form independent of p for the integral I^i , one has to expand the upper limits of all $I_n^{\theta(1)}, I_n^{\theta(2)}, \dots, I_n^{\theta(i)}$ around ϵ^{p-1} to enough orders and the same thing occurs for the lower limits of all $I_f^{\theta(1)}, I_f^{\theta(2)}, \dots, I_f^{\theta(i)}$ around ϵ^p . Now let's do this step by step.

The radial integrals at the next-to-leading order are analytically obtained as

$$I_n^{\theta(1)} = \int_{x_n}^{\epsilon^{p-1}} \frac{q^2 - 4(1 + 2\lambda x^2 + x^3)}{2\mathcal{R}_n^{3/2}} dx = \mathcal{F}_n^{\theta(1)}(\epsilon^{p-1}) - \mathcal{F}_n^{\theta(1)}(x_n), \quad (3.16)$$

with

$$\begin{aligned} \mathcal{F}_n^{\theta(1)}(x) = & \frac{1}{8\lambda^2 q^5 (q^2 - 4) \sqrt{\mathcal{R}_n}} \left[q^9 x - 4q^7 (x - \lambda) + 16\lambda q^5 (-\lambda x^2 + 2\lambda^2 x - 1) + 64\lambda^2 q^3 (-4\lambda^2 + x^2 - 9\lambda x) \right. \\ & \left. - 32\lambda^3 (q^4 - 10q^2 + 24) \sqrt{\mathcal{R}_n} \log \left(4\lambda + q^2 x + q\sqrt{\mathcal{R}_n} \right) + 768\lambda^3 q (\lambda + 2x) \right], \end{aligned} \quad (3.17)$$

and

$$I_f^{\theta(1)} = \int_{\epsilon^p}^{r_f} -\frac{4(\lambda r(r+1))}{\mathcal{R}_f^{3/2}} dr = \mathcal{F}_f^{\theta(1)}(r_f) - \mathcal{F}_f^{\theta(1)}(\epsilon^p), \quad (3.18)$$

with

$$\begin{aligned} \mathcal{F}_f^{\theta(1)}(r) = & \frac{4\lambda}{q^5 (q^2 - 4) r \sqrt{\mathcal{R}_f}} \left[- (q^4 - 10q^2 + 24) r \sqrt{\mathcal{R}_f} \log \left(\frac{q\sqrt{\mathcal{R}_f} + q^2 r + 2r^2}{r^2} \right) + 12qr(r+4) \right. \\ & \left. + q^5 (r-1) - 2q^3 (2r^2 + 9r - 2) \right]. \end{aligned} \quad (3.19)$$

As before, both $\mathcal{F}_n^{\theta(1)}(\epsilon^{p-1})$ and $\mathcal{F}_f^{\theta(i)}(\epsilon^p)$ depend on the specific value of p , but via the MAE, those p -dependent terms are properly canceled out with higher order \mathcal{F} functions. Then one can extract the p -independent terms

$$I^{\theta(1)} = \mathcal{F}_f^{\theta(1)}(r_f) - \mathcal{F}_n^{\theta(1)}(x_n) + \frac{4\lambda (q^2 - 6)}{q^5} \log \epsilon - \frac{8\lambda (q^2 - 6) \log(2q^2)}{q^5} + \frac{8\lambda (q^4 - 16q^2 + 40)}{q^5 (q^2 - 4)} + \frac{q}{8\lambda^2}. \quad (3.20)$$

Now, let's move on to the next order of the ϵ expansion. The radial integrals at the next-to-next-to-leading order (NNLO) are analytically obtained as

$$\begin{aligned} I_n^{\theta(2)} &= \int_{x_n}^{\epsilon^{p-1}} \frac{3(q^2 - 4(x^3 + 2\lambda x^2 + 1))^2 - 4\mathcal{R}_n(-4\lambda + x^4 - 4\lambda^2 x^2)}{8\mathcal{R}_n^{5/2}} dx \\ &= \mathcal{F}_n^{\theta(2)}(\epsilon^{p-1}) - \mathcal{F}_n^{\theta(2)}(x_n), \end{aligned} \quad (3.21)$$

and

$$\begin{aligned} I_f^{\theta(2)} &= \int_{\epsilon^p}^{r_f} \frac{2\lambda^2 (r+1)r^2 (q^2(r-1) + r^3 + 3r^2 + 8r + 12)}{\mathcal{R}_f^{5/2}} dr \\ &= \mathcal{F}_f^{\theta(2)}(r_f) - \mathcal{F}_f^{\theta(2)}(\epsilon^p), \end{aligned} \quad (3.22)$$

with

$$\begin{aligned}
\mathcal{F}_n^{\theta(2)}(x) = & \frac{1}{64\lambda^4 q^8 (q^2 - 4)^2 \mathcal{R}_n^{3/2}} \left[q^{18} x^3 + 2q^{16} x (3\lambda^2 - 4x^2 + 6\lambda x) + 8q^{14} (3\lambda^3 + 2x^3 - 12\lambda x^2 - 3\lambda^2 x) \right. \\
& - 16\lambda q^{12} (14\lambda^2 + \lambda^3 x^5 + (8\lambda^5 - 4\lambda^2) x^3 - 12(\lambda^3 + 1) x^2 + (6\lambda - 8\lambda^4) x) \\
& - 64\lambda^2 q^{10} (-10\lambda - 5\lambda^2 x^5 - 27\lambda^3 x^4 + 4\lambda(3\lambda^3 + 2) x^3 + 8\lambda^2(\lambda^3 + 3) x^2 + 2(4\lambda^6 + 8\lambda^3 - 3) x) \\
& + 256\lambda^3 q^8 (8\lambda^6 - 7\lambda x^5 - 75\lambda^2 x^4 + (418\lambda^3 + 4) x^3 + 4(37\lambda^3 + 3) \lambda x^2 + (13\lambda^3 + 8) \lambda^2 x - 2) \\
& + 1024\lambda^4 q^6 (109\lambda^5 + 3x^5 + 69\lambda x^4 - 1032\lambda^2 x^3 + 154\lambda^3 x^2 + 523\lambda^4 x) \\
& - 12288\lambda^5 q^4 (111\lambda^4 + 7x^4 - 306\lambda x^3 + 364\lambda^2 x^2 + 477\lambda^3 x) \\
& \left. + 81920\lambda^6 q^2 (65\lambda^3 - 56x^3 + 246\lambda x^2 + 267\lambda^2 x) - 6881280\lambda^7 (\lambda + 2x)^2 \right] \\
& + \frac{1}{q^9} \lambda^2 (2q^6 + 27q^4 - 600q^2 + 1680) \log \left(4\lambda + q^2 x + q\sqrt{\mathcal{R}_n} \right), \tag{3.23}
\end{aligned}$$

$$\begin{aligned}
\mathcal{F}_f^{\theta(2)}(r) = & \frac{\lambda^2}{q^9} \left[\frac{q\sqrt{\mathcal{R}_f}}{r} \left(\frac{(q^2 - 12) q^2}{r^2} + \frac{264 - 62q^2}{r} + \frac{8r^4 q^2 (q^6 - q^4(4r + 21) + q^2(22r + 96) - 32(r + 4))}{(q^2 - 4) \mathcal{R}_f^2} \right) \right. \\
& \left. + \frac{2(q^{10} + q^8(1 - 2r) - 2q^6(39r + 238) + 8q^4(119r + 568) - 64q^2(57r + 244) + 4608(r + 4))}{(q^2 - 4)^2 (q^2 + r(r + 4))} \right) \\
& - (2q^6 + 27q^4 - 600q^2 + 1680) \log \frac{q^2 r + q\sqrt{\mathcal{R}_f} + 2r^2}{r^2} \Big]. \tag{3.24}
\end{aligned}$$

Then those p -independent terms are obtained as

$$\begin{aligned}
I^{\theta(2)} = & \mathcal{F}_f^{\theta(2)}(r_f) - \mathcal{F}_n^{\theta(2)}(x_n) - \frac{\lambda^2 (\log \epsilon - 2 \log 2q^2)}{q^9} (2q^6 + 27q^4 - 600q^2 + 1680) \\
& + \frac{q^3}{64\lambda^4} + \frac{1}{\lambda q^3} + \frac{-4q^{10} - 21q^8 + 2576q^6 - 24288q^4 + 83712q^2 - 99584}{q^9 (q^2 - 4)^2} \lambda^2. \tag{3.25}
\end{aligned}$$

It is straightforward to push the calculation to the next order. So in the following we just list the results of $I^{(3)}$ and omit the details. At the NNNLO of the ϵ expansion, we have

$$\begin{aligned}
I^{\theta(3)} = & \mathcal{F}_f^{\theta(3)}(r_f) - \mathcal{F}_n^{\theta(3)}(x_n) \\
& + \frac{-591360\lambda^3 + q^{10} + 24(4\lambda^3 - 3)q^8 - 80(\lambda^3 - 3)q^6 - 43680\lambda^3 q^4 + 322560\lambda^3 q^2}{4q^{13}} (\log \epsilon - 2 \log 2q^2) \\
& + \frac{1}{384\lambda^6 q^{13} (q^2 - 4)^3} \left(13974372352\lambda^9 + q^{24} - 12q^{22} + 9093513216\lambda^9 q^4 - 17877958656\lambda^9 q^2 \right. \\
& + 24(\lambda^3 + 2)q^{20} - 48\lambda^3(11\lambda^3 - 36)q^{16} - 3072\lambda^6(3665\lambda^3 + 908)q^{10} + 36864\lambda^6(7595\lambda^3 + 193)q^8 \\
& - 16(6\lambda^6 - 21\lambda^3 - 4)q^{18} - 16384\lambda^6(139750\lambda^3 + 417)q^6 + 192\lambda^3(128\lambda^6 - 169\lambda^3 - 20)q^{14} \\
& \left. - 512\lambda^3(955\lambda^6 - 960\lambda^3 - 6)q^{12} \right), \tag{3.26}
\end{aligned}$$

where

$$\begin{aligned} \mathcal{F}_n^{\theta(3)}(x) = & \frac{1}{384q^{13}} \left[\frac{1}{\lambda^6 (q^2 - 4)^3 \mathcal{R}_n^{5/2}} \left(x^5 q^{29} + 2x^3 (-6x^2 + 10\lambda x + 5\lambda^2) q^{27} + \dots \right) \right. \\ & - 96 (-591360\lambda^3 + q^{10} + 24 (4\lambda^3 - 3) q^8 - 80 (\lambda^3 - 3) q^6 - 43680\lambda^3 q^4 + 322560\lambda^3 q^2) \\ & \left. \times \log \left(4\lambda + q\sqrt{\mathcal{R}_n} + q^2 x \right) \right], \end{aligned} \quad (3.27)$$

and

$$\begin{aligned} \mathcal{F}_f^{\theta(3)}(r) = & \frac{1}{12q^{13}} \left[\frac{q\sqrt{\mathcal{R}_f}}{r} \left(-\frac{32\lambda^3 q^4 (3q^2 - 20)}{r^3} + \dots \right) \right. \\ & + 3 (-591360\lambda^3 + q^{10} + 24 (4\lambda^3 - 3) q^8 - 80 (\lambda^3 - 3) q^6 - 43680\lambda^3 q^4 + 322560\lambda^3 q^2) \\ & \left. \times \log \frac{q^2 r + q\sqrt{\mathcal{R}_f + 2r^2}}{r^2} \right]. \end{aligned} \quad (3.28)$$

We find that the \mathcal{F} functions at this order is too lengthy to be list even in the appendix, so we just put them in the ancillary *Mathematica* files.

With the above expressions in hand, we are able to define a sum function as

$$S_\omega^{(i)} = \sum_{k=0}^i I^{\omega(k)} \epsilon^k \quad (3.29)$$

where, $i \in \mathbb{N}$ and $\omega \in \{\theta, \phi, t\}$. For example, we have

$$S_\theta^{(3)} = \sum_{k=0}^3 I^{\theta(k)} \epsilon^k = I^{\theta(0)} + I^{\theta(1)} \epsilon + I^{\theta(2)} \epsilon^2 + I^{\theta(3)} \epsilon^3, \quad (3.30)$$

which could be viewed as an analytical approximation for the radial integrals I^θ in Eq. (3.1).

In addition, in order to examine the accuracy of the approximate functions $S_\omega^{(i)}$, we would like to introduce the corresponding relative error functions as

$$\delta_\omega^{(i)} = \frac{|S_\omega^{(i)} - I^\omega|}{I^\omega}, \quad (3.31)$$

where I^ω denotes the exact value of the radial integrals of the $r - \omega$ motion.

On the other hand, to choose a suitable value of r_n , we note that the ISCO can be expanded in ϵ , which in terms of the coordinates (2.16) is given by

$$r_{ISCO} = 2^{1/3} \epsilon + \frac{7}{2^{1/3} 4} \epsilon^2 + \frac{15}{32} \epsilon^3 + \mathcal{O}(\epsilon^4). \quad (3.32)$$

One can see that the leading order of r_{ISCO} is $\mathcal{O}(\epsilon)$, so if the emitter is moving on the ISCO then the light ray can extend to the far region. Without loss of generality, here and in the subsequent sections

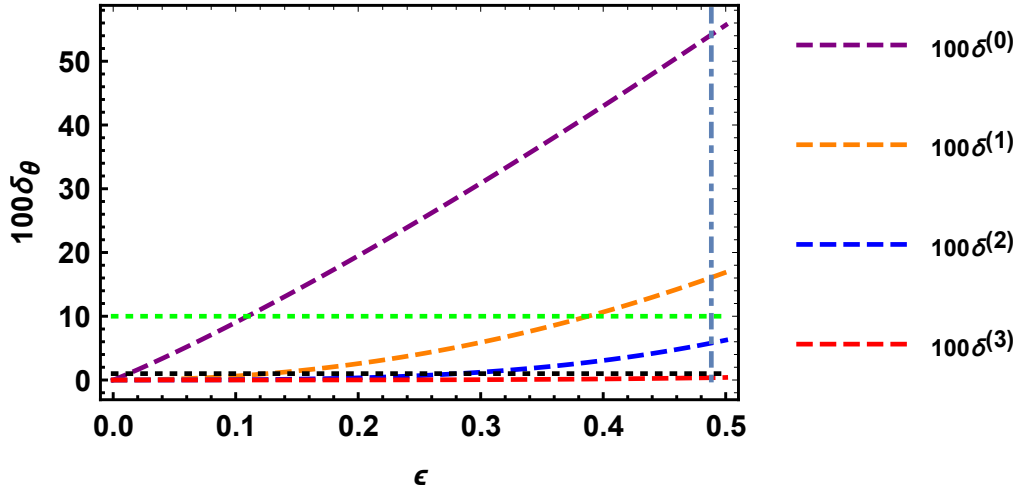


Figure 1: The relative error function $\delta_\theta^{(i)}$ with respect to ϵ for $q = \sqrt{3}$ and $\lambda = 1/2$. The green and black dotted horizontal lines are $\delta_\theta = 10\%$ and $\delta_\theta = 1\%$, respectively. The grey dot-dashed vertical line is $\epsilon = 0.488$ which corresponds to $a = 0.94$. For simplicity, we drop the subscript θ of the labels $\delta^{(i)}$ of the lines without any misunderstanding.

we take $r_n = 2^{1/3}\epsilon$, $r_f = 100$ for the examination of the analytically approximate expressions for the radial integrals and we give the numerical results of $\delta_\theta^{(i)}$ in Fig. 1 at $q = \sqrt{3}$ and $\lambda = 1/2$.

From this figure, we have to include the contributions up to the NNNLO term, i.e. $I^{\theta(3)}$ at least if we want to study the non-extremal Kerr black hole with $a = 0.94$ ($\epsilon = 0.488$) and retain the error within 1%. If we can tolerate an error of no more than 10 percent, pushing the results to the NNLO is enough. On the other hand, if only the leading term participates in the contribution, to retain the error within 1%, ϵ has to be smaller than 0.013, which means a has to be larger than 0.999999. Even if we make the error to less demanding standards, for example, the final results can have been put out by as much as 10%, ϵ has to be smaller than 0.12. Hence, in this sense, when q is much bigger than ϵ , the higher corrections could help the theoretical results closer to the observations of real black holes, such as M87*.

On the other hand, we also draw the pictures in Fig. 2 for $q = \lambda = 1/2$. From this graph, we can find $\epsilon \leq 0.0018$ if we allow the error to be within 10%, and the higher order terms could have advantages. However, if ϵ goes a little bigger, the higher order terms turn out to make things worse rather than better. This can be explained as follows. As we mentioned in the previous section, in the near-horizon region $r \simeq r_n \simeq \epsilon$ the validity of the expansion in ϵ requires that the parameter in the radial function $R(r)$ much larger than ϵ . In this case, the shifted Carter constant q cannot take a small value if ϵ is not very small. On the other hand, the behavior in the far region $r \gg \epsilon$ is much better, in this case the validity of the high spin expansion is independent of the value of ϵ .

Given all this, we conclude that the higher order terms can not only make those approximations more accurate, but also make it possible to calculate the radial integrals of null geodesics in the $r-\theta$ motion for $a \simeq 0.9$ when q is large. But for a small q , ϵ has to be very small and it's impossible

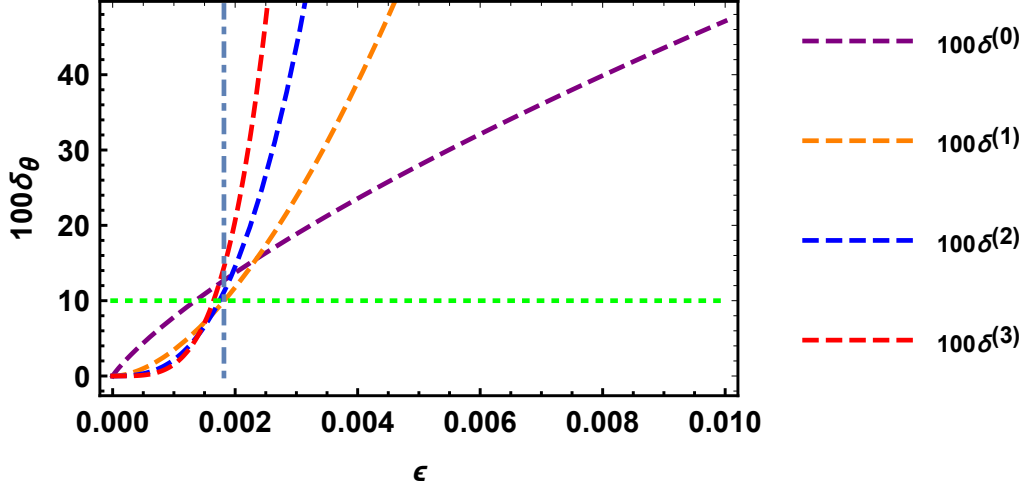


Figure 2: The relative error function $\delta_\theta^{(i)}$ with respect to ϵ for $q = \lambda = 1/2$. The green dotted horizon line is $\delta_\theta = 10\%$. The grey dot-dashed vertical line is $\epsilon = 0.0018$ which corresponds to $a = 0.999999997$. For simplicity, we drop the subscript θ of the labels $\delta^{(i)}$ of the lines.

to extend to the case Kerr black hole is not near extreme whether the higher orders are considered or not.

Nevertheless, the story is not complete, we still need to check the radial integrals of the $r - \phi$ and $r - t$ motion.

4 The radial integral for the $r - \phi$ motion

In this section, we pay our attention to the radial integral

$$I^\phi = \int_{r_n}^{r_f} \frac{\Phi}{(r^2 - \epsilon^3)\sqrt{R}} dr, \quad (4.1)$$

for the $r - \phi$ motion. As before, this integral can be separated into

$$I^\phi = I_n^\phi + I_f^\phi, \quad (4.2)$$

with

$$I_n^\phi = \int_{r_n}^{\epsilon^p} \frac{\Phi}{(r^2 - \epsilon^3)\sqrt{R}} dr, \quad I_f^\phi = \int_{\epsilon^p}^{r_f} \frac{\Phi}{(r^2 - \epsilon^3)\sqrt{R}} dr. \quad (4.3)$$

Then the integrals in the two regions can be analytically performed respectively in the high spin expansion and then via the matched asymptotic expansion method the solution in the whole region can be obtained.

At LO, we have

$$I_n^{\phi(0)} = \mathcal{F}_n^{\phi(0)}(\epsilon^{p-1}) - \mathcal{F}_n^{\phi(0)}(x_n), \quad (4.4)$$

and

$$I_f^{\phi(0)} = \mathcal{F}_f^{\phi(0)}(r_f) - \mathcal{F}_f^{\phi(0)}(\epsilon^p), \quad (4.5)$$

where

$$\mathcal{F}_n^{\phi(0)}(x) = \frac{3 \log(4\lambda + q\sqrt{\mathcal{R}_n} + q^2x)}{q} - 2 \log \frac{2\lambda + \sqrt{q^2x^2 + 4\lambda(\lambda + 2x)} + 2x}{x}, \quad (4.6)$$

$$\mathcal{F}_f^{\phi(0)}(r) = -\frac{3}{q} \log \frac{q\sqrt{\mathcal{R}_f} + q^2r + 2r^2}{r^2} + 2 \log \frac{\sqrt{\mathcal{R}_f} + r^2 + 2r}{r} + \frac{\sqrt{\mathcal{R}_f}}{r}. \quad (4.7)$$

The matching in the overlap region (2.23) with the integrals at higher orders of ϵ cancels the p -dependent terms and gives

$$I^{\phi(0)} = \mathcal{F}_f^{\phi(0)}(r_f) - \mathcal{F}_n^{\phi(0)}(x_n) + \frac{6 \log 2q^2}{q} - \frac{3 \log \epsilon}{q} - q - 4 \log(q + 2). \quad (4.8)$$

At NLO, similarly we have

$$I_n^{\phi(1)} = \mathcal{F}_n^{\phi(1)}(\epsilon^{p-1}) - \mathcal{F}_n^{\phi(1)}(x_n), \quad (4.9)$$

and

$$I_f^{\phi(1)} = \mathcal{F}_f^{\phi(1)}(r_f) - \mathcal{F}_f^{\phi(1)}(\epsilon^p). \quad (4.10)$$

Then the integral in the whole region at this order is given by

$$\begin{aligned} I^{\phi(1)} &= \mathcal{F}_f^{\phi(1)}(r_f) - \mathcal{F}_n^{\phi(1)}(x_n) - \frac{4\lambda(q^2 - 6)(q^2 - 3)(\log \epsilon - 2 \log 2q^2)}{q^5} \\ &\quad + \frac{7680\lambda^3 + 3q^8 - 4(8\lambda^3 + 3)q^6 + 1024\lambda^3q^4 - 5376\lambda^3q^2}{8\lambda^2q^5(q^2 - 4)}. \end{aligned} \quad (4.11)$$

From now on, we move all the higher order $\mathcal{F}_n^{\phi(i)}(x)$ and $\mathcal{F}_f^{\phi(i)}(r)$ functions with $i = 1, 2, 3$ to the appendix A. In the same way, at NNLO, we find

$$I_n^{\phi(2)} = \mathcal{F}_n^{\phi(2)}(\epsilon^{p-1}) - \mathcal{F}_n^{\phi(2)}(x_n), \quad (4.12)$$

and

$$I_f^{\phi(2)} = \mathcal{F}_f^{\phi(2)}(r_f) - \mathcal{F}_f^{\phi(2)}(\epsilon^p). \quad (4.13)$$

The radial integral at this order is given by

$$\begin{aligned} I^{\phi(2)} &= \mathcal{F}_f^{\phi(2)}(r_f) - \mathcal{F}_n^{\phi(2)}(x_n) + \frac{3\lambda^2(\log \epsilon - 2 \log 2q^2)}{q^9} (4q^6 - 187q^4 + 1080q^2 - 1680) \\ &\quad + \frac{1}{64\lambda^4q^9(q^2 - 4)^2} \left(-19120128\lambda^6 + 3q^{16} - 24q^{14} - 9029632\lambda^6q^4 + 21430272\lambda^6q^2 \right. \\ &\quad \left. - 64\lambda^3(\lambda^3 - 27)q^{10} - 64\lambda^3(1975\lambda^3 + 72)q^8 + 1024\lambda^3(1673\lambda^3 + 3)q^6 \right. \\ &\quad \left. + 16(8\lambda^6 - 12\lambda^3 + 3)q^{12} \right). \end{aligned} \quad (4.14)$$

Again, at NNNLO, we obtain

$$I_n^{\phi(3)} = \mathcal{F}_n^{\phi(3)}(\epsilon^{p-1}) - \mathcal{F}_n^{\phi(3)}(x_n), \quad (4.15)$$

and

$$I_f^{\phi(3)} = \mathcal{F}_f^{\phi(3)}(r_f) - \mathcal{F}_f^{\phi(3)}(\epsilon^p). \quad (4.16)$$

The integral is then given by

$$\begin{aligned} I^{\phi(3)} &= \mathcal{F}_f^{\phi(3)}(r_f) - \mathcal{F}_n^{\phi(3)}(x_n) \\ &+ \frac{\log \epsilon - 2 \log 2q^2}{4q^{13}} \left(-1774080\lambda^3 - 2q^{12} - 381920\lambda^3 q^4 + 1451520\lambda^3 q^2 \right. \\ &+ (99 - 32\lambda^3) + q^{10} + 168(2\lambda^3 - 3)q^8 + 720(43\lambda^3 + 1)q^6 \left. \right) \\ &+ \frac{1}{384\lambda^6 q^{13} (q^2 - 4)^3} \left(41923117056\lambda^9 + 3q^{24} - 64977371136\lambda^9 q^2 \right. \\ &+ 4(2\lambda^3 - 9)q^{22} - 24(7\lambda^3 - 6)q^{20} - 147456\lambda^6(94346\lambda^3 + 139)q^6 + 41480355840\lambda^9 q^4 \\ &- 48(14\lambda^6 - 23\lambda^3 + 4)q^{18} - 1024\lambda^6(232825\lambda^3 + 16092)q^{10} + 12288\lambda^6(208571\lambda^3 + 2361)q^8 \\ &+ 192\lambda^3(1616\lambda^6 - 3611\lambda^3 - 12)q^{14} - 16\lambda^3(576\lambda^6 - 2829\lambda^3 + 140)q^{16} \\ &\left. + 1536\lambda^3(4489\lambda^6 + 3072\lambda^3 + 6)q^{12} \right). \quad (4.17) \end{aligned}$$

With the above expressions, we have the final result,

$$S_\phi^{(i)} = \sum_{k=0}^i I^{\phi(k)} \epsilon^k, \quad (4.18)$$

and

$$\delta_\phi^{(i)} = \frac{|S_\phi^{(i)} - I^\phi|}{I^\phi}. \quad (4.19)$$

Also, we plot the relative error functions in Fig. 3 and 4 for $q = \sqrt{3}$ and $\lambda = 1/2$ and $q = \lambda = 1/2$, respectively.

From these figures, we find that it's better to include the contributions of higher order terms only if ϵ is small enough, no matter q is large or small. When the deviation ϵ gets to a certain size and then increases, considering a higher order will raise the relative error, that is, the leading term gives the best approximate values of the original integrals. In addition, we find the analytical expressions are not sensitive to ϵ for a large q , even ϵ increases to 0.9, the approximate results are still controlled within 1% error. However, turning to the small q and looking at the the best analytical expression, that is, the leading term, the relative error can quickly exceed 10 percent corresponding to $\epsilon = 0.118$ and $a = 0.9992$ which is far from the real rotating black hole in our universe.

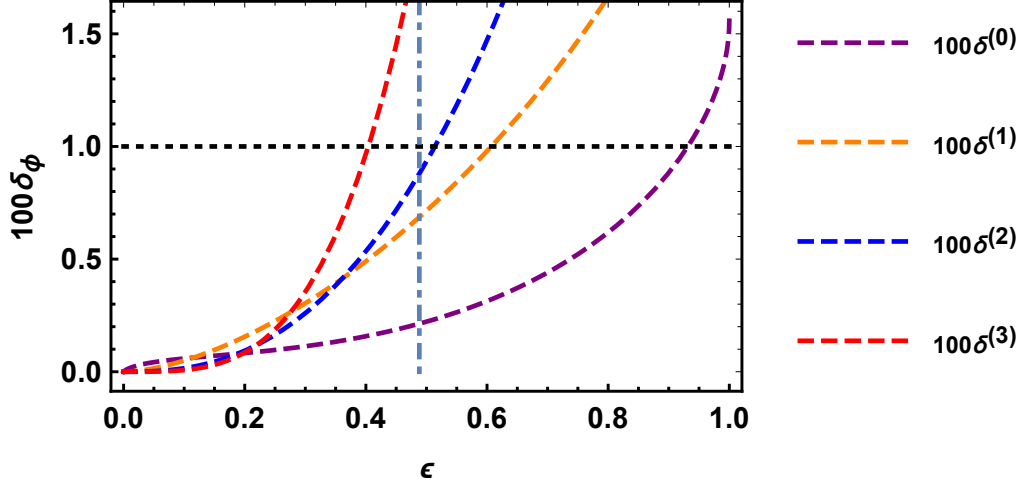


Figure 3: The relative error function $\delta_\phi^{(i)}$ with respect to ϵ for $q = \sqrt{3}$ and $\lambda = 1/2$. Also, the black dotted horizon line is $\delta_\theta = 1\%$. The grey dot-dashed vertical line is $\epsilon = 0.488$ which corresponds to $a = 0.94$. For simplicity, we drop the subscript ϕ of the labels $\delta^{(i)}$ of the lines.

5 The radial integral for the $r - t$ motion

In this section, let's finish our calculation with the radial integral

$$I^t = \int_{r_n}^{r_f} \frac{T(r)}{(r^2 - \epsilon^3)\sqrt{R(r)}} dr, \quad (5.1)$$

for the $r - t$ motion, which can be separated into

$$I^t = I_n^t + I_f^t, \quad (5.2)$$

with

$$I_n^t = \int_{r_n}^{\epsilon^p} \frac{T}{(r^2 - \epsilon^3)\sqrt{R}} dr, \quad I_f^t = \int_{\epsilon^p}^{r_f} \frac{T}{(r^2 - \epsilon^3)\sqrt{R}} dr. \quad (5.3)$$

At LO, we have

$$I_n^{t(0)} = \mathcal{F}_n^{t(0)}(\epsilon^{p-1}) - \mathcal{F}_n^{t(0)}(x_n), \quad (5.4)$$

and

$$I_f^{t(0)} = \mathcal{F}_f^{t(0)}(r_f) - \mathcal{F}_f^{t(0)}(\epsilon^p), \quad (5.5)$$

where

$$\mathcal{F}_n^{t(0)}(x) = -\frac{\sqrt{\mathcal{R}_n}}{\lambda x} \frac{1}{\epsilon}, \quad (5.6)$$

$$\begin{aligned} \mathcal{F}_f^{t(0)}(r) &= \frac{\sqrt{\mathcal{R}_f}}{r} \left(1 - \frac{4}{q^2 r}\right) - \frac{(7q^2 - 8)}{q^3} \log \left(\frac{q^2 r + q\sqrt{\mathcal{R}_f} + 2r^2}{r^2} \right) \\ &+ 2 \log \left(\frac{r^2 + 2r + \sqrt{\mathcal{R}_f}}{r} \right). \end{aligned} \quad (5.7)$$

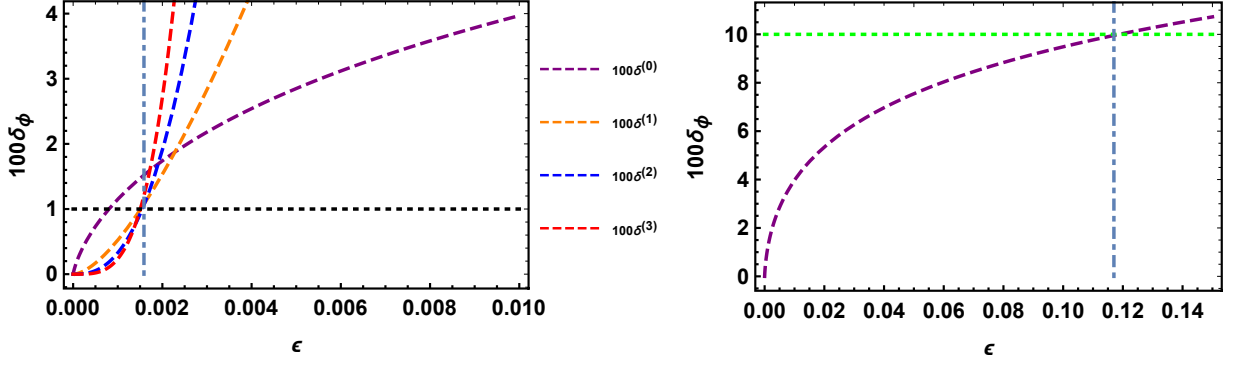


Figure 4: The relative error function $\delta_\phi^{(i)}$ with respect to ϵ for $q = \lambda = 1/2$. In the left graph, the green and black dotted horizontal lines are $\delta_\theta = 10\%$ and $\delta_\theta = 1\%$, respectively. The grey dot-dashed vertical line is $\epsilon = 0.488$ which corresponds to $a = 0.94$. For simplicity, we drop the subscript ϕ of the labels $\delta^{(i)}$ of the lines. In the right graph, we replot $\delta_\phi^{(0)}$ in the range $\epsilon \in (0, 0.15)$ to show the maximum value of ϵ to keep the fault tolerance is less than 10%.

Then the integral is given by

$$I^{t(0)} = \mathcal{F}_f^{t(0)}(r_f) - \mathcal{F}_n^{t(0)}(x_n) - \frac{q}{\lambda\epsilon}. \quad (5.8)$$

At NLO, we have

$$I_n^{t(1)} = \mathcal{F}_n^{t(1)}(\epsilon^{p-1}) - \mathcal{F}_n^{t(1)}(x_n), \quad (5.9)$$

and

$$I_f^{t(1)} = \mathcal{F}_f^{t(1)}(r_f) - \mathcal{F}_f^{t(1)}(\epsilon^p). \quad (5.10)$$

Then the integral is given by

$$I^{t(1)} = \mathcal{F}_f^{t(1)}(r_f) - \mathcal{F}_n^{t(1)}(x_n) + \frac{1}{\epsilon} \left(-\frac{q^3}{12\lambda^3} + \frac{24}{q^3} + \frac{(8 - 7q^2)(\log \epsilon - 2 \log 2q^2)}{q^3} - q - \frac{4}{q} - 4 \log(q + 2) \right). \quad (5.11)$$

Similar to the previous section, we have moved all the higher order $\mathcal{F}_n^{t(i)}(x)$ and $\mathcal{F}_f^{t(i)}(r)$ functions with $i = 1, 2, 3$ to the appendix A. At NNLO, we have

$$I_n^{t(2)} = \mathcal{F}_n^{t(2)}(\epsilon^{p-1}) - \mathcal{F}_n^{t(2)}(x_n), \quad (5.12)$$

and

$$I_f^{t(2)} = \mathcal{F}_f^{t(2)}(r_f) - \mathcal{F}_f^{t(2)}(\epsilon^p). \quad (5.13)$$

Then the integral is given by

$$\begin{aligned}
I^{t(2)} &= \mathcal{F}_f^{t(2)}(r_f) - \mathcal{F}_n^{t(2)}(x_n) \\
&+ \frac{6\lambda(\log \epsilon - 2 \log 2q^2)}{\epsilon q^7} (9q^4 - 52q^2 + 80) \\
&- \frac{1}{80\epsilon\lambda^5 q^7 (q^2 - 4)} \left(558080\lambda^6 + q^{14} - 4q^{12} - 30\lambda^3 q^{10} + 40(4\lambda^6 + \lambda^3) q^8 \right. \\
&\left. - 80\lambda^3 (163\lambda^3 - 4) q^6 + 136000\lambda^6 q^4 - 480000\lambda^6 q^2 \right). \tag{5.14}
\end{aligned}$$

At NNNLO, we have

$$I_n^{t(3)} = \mathcal{F}_n^{t(3)}(\epsilon^{p-1}) - \mathcal{F}_n^{t(3)}(x_n), \tag{5.15}$$

and

$$I_f^{t(3)} = \mathcal{F}_f^{t(3)}(r_f) - \mathcal{F}_f^{t(3)}(\epsilon^p), \tag{5.16}$$

Then the integral is given by

$$\begin{aligned}
I^{t(3)} &= \mathcal{F}_f^{t(3)}(r_f) - \mathcal{F}_n^{t(3)}(x_n) \\
&- \frac{3\lambda^2(\log \epsilon - 2 \log 2q^2)}{\epsilon q^{11}} (4q^8 + 183q^6 - 2640q^4 + 10640q^2 - 13440) \\
&- \frac{1}{448\epsilon\lambda^7 q^{11} (q^2 - 4)^2} \left(-1102839808\lambda^9 + q^{22} - 8q^{20} - 224\lambda^3 q^{16} + 1399078912\lambda^9 q^2 \right. \\
&+ (7\lambda^3 + 16) q^{18} + 448\lambda^6 (1263\lambda^3 + 136) q^{10} - 21504\lambda^6 (841\lambda^3 + 5) q^8 - 692142080\lambda^9 q^4 \\
&\left. - 112\lambda^3 (8\lambda^6 - 13\lambda^3 - 13) q^{14} + 448\lambda^3 (57\lambda^6 - 35\lambda^3 - 6) q^{12} + 14336\lambda^6 (11485\lambda^3 + 6) q^6 \right). \tag{5.17}
\end{aligned}$$

As we did before, we gave two examples for the large and small parameter q in Fig. 5 and 6. For the small case, we choose $q = \lambda = 1/2$ again, while unlike the other motions we choose $q = 3/2$ and $\lambda = 1/2$ to take a glance at the difference that changing q makes when q is relatively large.

From Fig. 5, we find that the expressions including the leading and next leading terms are the best approximations of the original integrals when ϵ is large to $1/2$. The relative error is always less than 1% in the range $\epsilon \in (0, 1/2)$. Compared with the results of the other motions, we conclude that it's not the more orders, we're thinking about, the better. Turning to the small q , the approximate expressions are also shown to apply only when the ϵ is very small, that is, the high spin expansion and MAE methods don't work well if one wants to find analytical expressions instead of the numerical calculations approximatively.

6 Summary

Due to the emergence of an enhanced symmetry of the near-horizon geometry of the (near-) extreme Kerr black hole, the radial integrals of the null geodesic equations can be analytically

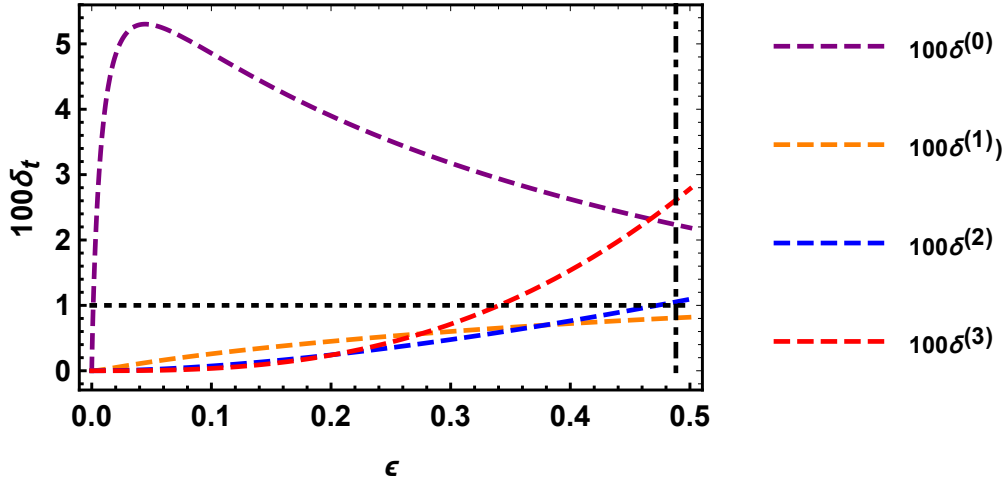


Figure 5: The relative error function $\delta_t^{(i)}$ with respect to ϵ for $q = 3/2$ and $\lambda = 1/2$. The black dotted horizontal line is $\delta_\theta = 1\%$, respectively. The grey dot-dashed vertical line is $\epsilon = 0.488$ which corresponds to $a = 0.94$. For simplicity, we drop the subscript ϕ of the labels $\delta^{(i)}$ of the lines.

obtained [8]. Following the method proposed in [8] and [12], we extended the computation of the radial integrals of null geodesics to higher orders in ϵ , where ϵ is a very small parameter characterizing the spin of the Kerr black hole deviating from extremity $a = M$.

Considering the null geodesics that begin from the near-horizon region $r_n \ll 1$ and end at the far region $r_f \gg \epsilon$. We first expanded the radial integrals in terms of ϵ for both regions, in particular, as pointed out in [12], we also made the change of variable $x = r/\epsilon$ in the near-horizon region to ensure the validity of the expansion. By employing the method of MAE, we obtained the analytical expressions of the radial integrals up to NNNLO in ϵ . The results of the first four orders for $r - \theta$ motion can be found in Eqs. (3.15)-(3.26). We showed the expressions for $r - \phi$ motion in Eqs. (4.8)-(4.17). And for $r - t$ motion, the results are given in Eqs. (5.8)-(5.17). As expected, our results of the leading term are the same with those in [8, 12].

By comparing these analytical expressions with the numerical evaluations of the exact integrals, we investigated the effectiveness of the high spin expansion method. To achieve this, we defined the sum function in Eq. (3.29) and the relative error function in Eq. (3.31). We found that the validity of the high spin expansion requires that $q \gg \epsilon$. For a large q , the analytical expressions behave very well, thus the results may be applied to the study of the electromagnetic signature in the spacetime of M87* black hole whose spin is supposed to be $a \simeq 0.9M$. However, for a small q , to retain a satisfactory precision our results show that ϵ has to be very small. In this case, the high spin expansion method can only apply to (near-) extreme black holes, excluding black holes like M87*. New methods have to be developed to solve this problem. Nevertheless, when it comes the situation with a large q , the results from the high spin expansion method may be a good choice due to their analyticity and accuracy.

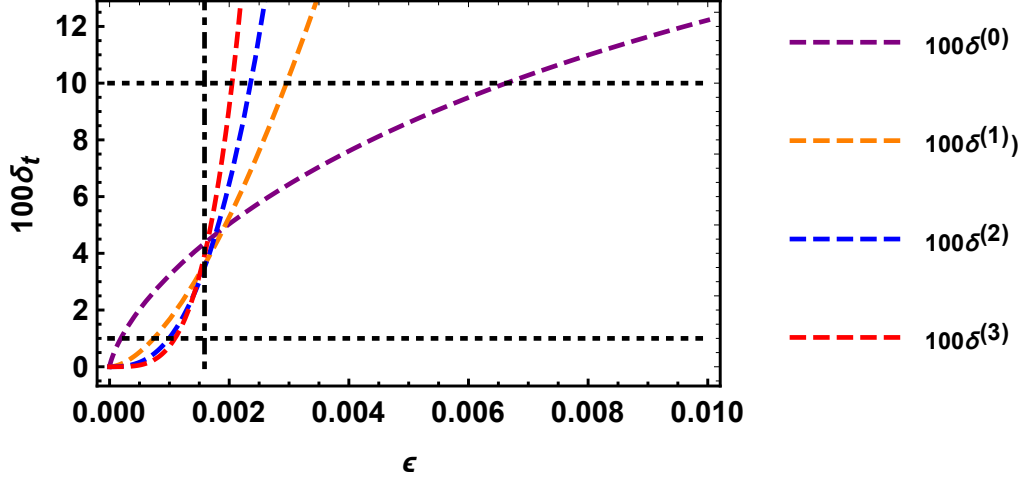


Figure 6: The relative error function $\delta_t^{(i)}$ with respect to ϵ for $q = \lambda = 1/2$. The black dotted horizon lines are $\delta_\theta = 10\%$ and $\delta_\theta = 1\%$, respectively. The black dot-dashed vertical line is $\epsilon = 0.0016$ which corresponds to $a = 0.999999998$. For simplicity, we drop the subscript ϕ of the labels $\delta^{(i)}$ of the lines.

Acknowledgments

We thank Jiang Long and Haopeng Yan for useful discussions. The work is in part supported by NSFC Grant No. 11335012, No. 11325522 and No. 11735001. MG and PCL are also supported by NSFC Grant No. 11947210. And MG is also funded by China National Postdoctoral Innovation Program 2019M660278.

A Details of \mathcal{F}^ϕ and \mathcal{F}^t functions

In this appendix, we show all the higher order $\mathcal{F}_n^{\phi(i)}(x)$ and $\mathcal{F}_f^{\phi(i)}(r)$ functions of the radial integrals for the $r - \phi$ motion and $\mathcal{F}_n^{t(i)}(x)$ and $\mathcal{F}_f^{t(i)}(r)$ functions of the radial integrals for the $r - t$ motion:

$$\begin{aligned}
\mathcal{F}_n^{\phi(1)}(x) = & \frac{1}{8\lambda^2 q^5 (q^2 - 4) x^2 \sqrt{\mathcal{R}_n}} \left(3q^9 x^3 + 2304\lambda^3 q x^2 (\lambda + 2x) + 192\lambda^2 q^3 x^2 (-8\lambda^2 + x^2 - 17\lambda x) \right. \\
& + 4q^7 (-4\lambda^3 + 8\lambda^2 x^4 - 3x^3 + 3\lambda x^2 - 4\lambda^2 x) + 16\lambda q^5 (4\lambda^2 - 11\lambda x^4 + 34\lambda^2 x^3 \\
& \left. + (16\lambda^3 - 3) x^2 + 4\lambda x) + 32\lambda^3 (q^6 - 13q^4 + 54q^2 - 72) \sqrt{\mathcal{R}_n} x^2 \log \left(4\lambda + q^2 x + q\sqrt{\mathcal{R}_n} \right) \right),
\end{aligned} \tag{A.1}$$

$$\begin{aligned} \mathcal{F}_f^{\phi(1)}(r) &= -\frac{4\lambda(q^2-6)(q^2-3)}{q^5} \log \frac{q^2r + q\sqrt{\mathcal{R}_f} + 2r^2}{r^2} \\ &\quad + \frac{4\lambda(q^2-3)(q^4(r-1) - 2q^2(2r^2+9r-2) + 12r(r+4))}{q^4(q^2-4)\sqrt{\mathcal{R}_f}}, \end{aligned} \quad (\text{A.2})$$

$$\begin{aligned} \mathcal{F}_n^{\phi(2)}(x) &= \frac{1}{64\lambda^4q^8(q^2-4)^2x^4\mathcal{R}_n^{3/2}} \left(3q^{18}x^7 - 20643840\lambda^7x^4(\lambda+2x)^2 - 6q^{16}x^5(-3\lambda^2+4x^2-6\lambda x) \right. \\ &\quad - 12288\lambda^5q^4x^4(693\lambda^4+21x^4-1238\lambda x^3+2452\lambda^2x^2+2911\lambda^3x) - 245760\lambda^6q^2x^4(-89\lambda^3 \\ &\quad + 56x^3-342\lambda x^2-363\lambda^2x) + 1024\lambda^4q^6x^4(1391\lambda^5+9x^5+279\lambda x^4-6152\lambda^2x^3 \\ &\quad + 3918\lambda^3x^2+6153\lambda^4x) + 8q^{14}x^2(-12\lambda^5+4\lambda^4x^7+(6-24\lambda^3)x^5 \\ &\quad - 12\lambda(4\lambda^3+3)x^4-\lambda^2(16\lambda^3+9)x^3+9\lambda^3x^2-12\lambda^4x) - 16\lambda q^{12}(16\lambda^6+35\lambda^3x^9 \\ &\quad + 96\lambda^4x^8-12\lambda^2(2\lambda^3+9)x^7+4(8\lambda^6-37\lambda^3-9)x^6+2\lambda(52\lambda^3+9)x^5 \\ &\quad + 2\lambda^2(64\lambda^3+21)x^4+8\lambda^3(4\lambda^3-7)x^3-24\lambda^4x^2+48\lambda^5x) - 256\lambda^3q^8(16\lambda^4+37\lambda x^9 \\ &\quad + 465\lambda^2x^8-2(2279\lambda^3+6)x^7-4\lambda(\lambda^3-11)x^6+3\lambda^2(523\lambda^3+56)x^5 \\ &\quad + 2(152\lambda^6+64\lambda^3+3)x^4+8\lambda(4\lambda^3-1)x^3+24\lambda^2x^2+48\lambda^3x) \\ &\quad + 64\lambda^2q^{10}(32\lambda^5+55\lambda^2x^9+345\lambda^3x^8-12\lambda(109\lambda^3+6)x^7-8(52\lambda^5+\lambda^2)x^6 \\ &\quad + (-32\lambda^7+256\lambda^4+30\lambda)x^4+8\lambda^2(8\lambda^3-5)x^3+24\lambda^3x^2+96\lambda^4x) \\ &\quad \left. + (-48\lambda^6+304\lambda^3+18)x^5 \right) \\ &\quad - \frac{3\lambda^2 \log(4\lambda + q\sqrt{\mathcal{R}_n} + q^2x)}{q^9} (4q^6 - 187q^4 + 1080q^2 - 1680), \end{aligned} \quad (\text{A.3})$$

$$\begin{aligned} \mathcal{F}_f^{\phi(2)}(r) &= \frac{\lambda^2}{q^9} \left[\frac{\sqrt{q\mathcal{R}_f}}{r} \left(\frac{(11q^2-36)q^2}{r^2} + \frac{40q^4-394q^2+792}{r} \right) \right. \\ &\quad \left. - \frac{8r^4q^2(q^2-3)(q^6-q^4(4r+21)+q^2(22r+96)-32(r+4))}{(q^2-4)\mathcal{R}_f^2} \right] \end{aligned} \quad (\text{A.4})$$

$$\begin{aligned} &\quad - \frac{1}{(q^2-4)^2\mathcal{R}_f} \left(2r^2(q^{12}-2q^{10}(r+3)-q^8(56r+379)+2q^6(517r+2626)) \right. \\ &\quad \left. - 8q^4(753r+3400)+64q^2(235r+988)-13824(r+4) \right) \\ &\quad \left. + 3(4q^6-187q^4+1080q^2-1680) \log \left(\frac{q^2r + q\sqrt{\mathcal{R}_f} + 2r^2}{r^2} \right) \right], \end{aligned} \quad (\text{A.5})$$

$$\begin{aligned}
\mathcal{F}_n^{\phi(3)}(x) &= \frac{\log(4\lambda + q\sqrt{\mathcal{R}_n} + q^2x)}{4q^{13}} \left(1774080\lambda^3 + 2q^{12} + 381920\lambda^3q^4 - 1451520\lambda^3q^2 \right. \\
&\quad \left. + (32\lambda^3 - 99)q^{10} - 168(2\lambda^3 - 3)q^8 - 720(43\lambda^3 + 1)q^6 \right) \\
&\quad + \frac{1}{384\lambda^6q^{13}(q^2 - 4)^3\mathcal{R}_n^{5/2}x^6} \left(3q^{29}x^{11} + 174399160320\lambda^{11}qx^6(\lambda + 2x)^3 + \dots \right),
\end{aligned} \tag{A.6}$$

$$\begin{aligned}
\mathcal{F}_f^{\phi(3)}(r) &= \frac{\sqrt{\mathcal{R}_f}}{12q^{12}r} \left(\frac{32\lambda^3q^4(q^4 - 21q^2 + 60)}{r^3} + \dots \right) \\
&\quad - \frac{1}{4q^{13}} \log\left(\frac{q^2r + q\sqrt{\mathcal{R}_f} + 2r^2}{r^2}\right) \left(1774080\lambda^3 + 2q^{12} + (32\lambda^3 - 99)q^{10} + \dots \right),
\end{aligned} \tag{A.7}$$

$$\begin{aligned}
\mathcal{F}_n^{t(1)}(x) &= \frac{1}{12\lambda^3q^3\sqrt{\mathcal{R}_n}x^3\epsilon} \left(24\lambda^3q^3\sqrt{\mathcal{R}_n}x^3\log(x) + 12\lambda^3(7q^2 - 8)\sqrt{\mathcal{R}_n}x^3\log(4\lambda + q^2x + q\sqrt{\mathcal{R}_n}) \right. \\
&\quad \left. - q(q^6x^4 + 2\lambda q^4x^2(\lambda + 2x) + 8\lambda^2q^2(2\lambda^2 + 6\lambda x^4 - x^2 + 2\lambda x) - 96\lambda^3x^3(\lambda + 2x)) \right. \\
&\quad \left. + 24\lambda^3q^2\sqrt{\mathcal{R}_n}x^3\log(\sqrt{\mathcal{R}_n} + 2(\lambda + x)) \right),
\end{aligned} \tag{A.8}$$

$$\begin{aligned}
\mathcal{F}_f^{t(1)}(r) &= -\frac{2\lambda}{q^7(q^2 - 4)r\sqrt{\mathcal{R}_f}} \left(-2q^9r^2 + 2q^9r + q^9 + 8q^7r^3 + 51q^7r^2 - 32q^7r - 8q^7 \right. \\
&\quad \left. - 102q^5r^3 - 468q^5r^2 + 136q^5r + 16q^5 + 392q^3r^3 + 1648q^3r^2 - 160q^3r \right. \\
&\quad \left. - 3(9q^6 - 88q^4 + 288q^2 - 320)r\sqrt{\mathcal{R}_f}\log\left(\frac{q^2r + q\sqrt{\mathcal{R}_f} + 2r^2}{r^2}\right) - 480qr^3 - 1920qr^2 \right),
\end{aligned} \tag{A.9}$$

$$\begin{aligned}
\mathcal{F}_n^{t(2)}(x) = & -\frac{1}{80\lambda^5 q^6 (q^2 - 4) \mathcal{R}_n^{3/2} x^5 \epsilon} \left(q^{16} x^8 + 2q^{14} x^6 (3\lambda^2 - 2x^2 + 6\lambda x) + 614400\lambda^7 x^5 (\lambda + 2x)^2 \right. \\
& + 10240\lambda^6 q^2 x^5 (-49\lambda^3 + 40x^3 - 186\lambda x^2 - 201\lambda^2 x) - 6\lambda q^{12} x^4 (-\lambda^3 + 5\lambda^2 x^4 + 8x^3 - 4\lambda^2 x) \\
& + 7680\lambda^5 q^4 x^5 (17\lambda^4 + x^4 - 46\lambda x^3 + 56\lambda^2 x^2 + 73\lambda^3 x) - 8\lambda^2 q^{10} x^2 (-12\lambda^4 + 40\lambda^3 x^7 \\
& + 5\lambda (4\lambda^3 - 1) x^6 + 45\lambda^2 x^5 + (12 - 25\lambda^3) x^4 - 4\lambda (5\lambda^3 - 4) x^3 + 9\lambda^2 x^2 - 12\lambda^3 x) \\
& - 128q^6 \lambda^4 (8\lambda^4 + 55\lambda x^9 - 810\lambda^2 x^8 + 4\lambda (5\lambda^3 - 1) x^3 + 12\lambda^2 x^2 + 24\lambda^3 x \\
& + 5 (7\lambda^3 - 6) x^7 + 5\lambda (71\lambda^3 - 16) x^6 + 5\lambda^2 (16\lambda^3 + 3) x^5 + (60\lambda^3 + 3) x^4) \\
& + 32\lambda^3 q^8 (8\lambda^5 + 80\lambda^2 x^9 - 5 (59\lambda^3 - 2) x^8 - 5\lambda (32\lambda^3 - 3) x^7 - 5\lambda^2 (4\lambda^3 + 21) x^6 \\
& \left. + (4 - 5\lambda^3) x^5 + (60\lambda^4 + 9\lambda) x^4 + 4\lambda^2 (5\lambda^3 - 4) x^3 + 24\lambda^4 x) \right) \\
& - \frac{6\lambda \log(4\lambda + q^2 x + q\sqrt{\mathcal{R}_n})}{q^7 \epsilon} (9q^4 - 52q^2 + 80), \tag{A.10}
\end{aligned}$$

$$\begin{aligned}
\mathcal{F}_f^{t(2)}(r) = & -\frac{3\lambda^2 (4q^8 + 183q^6 - 2640q^4 + 10640q^2 - 13440)}{q^{11}} \log\left(\frac{q^2 r + q\sqrt{\mathcal{R}_f} + 2r^2}{r^2}\right) \\
& + \frac{\lambda^2 \sqrt{\mathcal{R}_f}}{q^{10} r} \left[\frac{8(q^2 - 4)q^4}{r^3} + \frac{(23q^4 - 268q^2 + 544)q^2}{r^2} + \frac{2(8q^6 - 445q^4 + 2564q^2 - 3936)}{r} \right. \\
& - \frac{8q^2 (q^{10} - 4q^8(r+7) + q^6(54r+275) - 18q^4(15r+68) + 32q^2(19r+80) - 512(r+4))}{(q^2 - 4)(q^2 + r(r+4))^2} \\
& - \frac{2}{(q^2 - 4)^2 (q^2 + r(r+4))} \left(q^{14} - 2q^{12}(r+9) + 98304(r+4) - q^{10}(20r+223) \right. \\
& \left. \left. + 2q^8(639r+3686) - 8q^6(1651r+8052) + 64q^4(917r+4080) - 512q^2(239r+1000) \right) \right], \tag{A.11}
\end{aligned}$$

$$\begin{aligned}
\mathcal{F}_n^{t(3)}(x) = & \frac{3\lambda^2 \log(4\lambda + q\sqrt{\mathcal{R}_n} + q^2 x)}{\epsilon q^{11}} (4q^8 + 183q^6 - 2640q^4 + 10640q^2 - 13440) \\
& + \frac{1}{448\epsilon \lambda^7 q^{10} (q^2 - 4)^2 x^7 \mathcal{R}_n^{5/2}} \left(4624220160\lambda^{11} x^7 (\lambda + 2x)^3 - q^{26} x^{12} + \dots \right), \tag{A.12}
\end{aligned}$$

$$\begin{aligned}
\mathcal{F}_f^{t(3)}(r) = & -\frac{1}{12q^{15}} \left[\frac{q\sqrt{\mathcal{R}_f}}{r} \left(-\frac{24\lambda^3 q^6 (q^4 - 24q^2 + 80)}{r^4} + \dots \right) \right. \\
& \left. + 3 \log\left(\frac{q^2 r + q\sqrt{\mathcal{R}_f} + 2r^2}{r^2}\right) \left(-15375360\lambda^3 + 2q^{14} - 91q^{12} + \dots \right) \right]. \tag{A.13}
\end{aligned}$$

The explicit form of the \mathcal{F} functions at the NNNLO can be found in the ancillary *Mathematica* files.

References

- [1] The Event Horizon Telescope (EHT), <http://eventhorizontelescope.org>
- [2] K. Akiyama *et al.* [Event Horizon Telescope Collaboration], “First M87 Event Horizon Telescope Results. I. The Shadow of the Supermassive Black Hole,” *Astrophys. J.* **875**, no. 1, L1 (2019) doi:10.3847/2041-8213/ab0ec7 [arXiv:1906.11238 [astro-ph.GA]].
- [3] K. Akiyama *et al.* [Event Horizon Telescope Collaboration], “First M87 Event Horizon Telescope Results. II. Array and Instrumentation,” *Astrophys. J.* **875**, no. 1, L2 (2019) doi:10.3847/2041-8213/ab0c96 [arXiv:1906.11239 [astro-ph.IM]].
- [4] K. Akiyama *et al.* [Event Horizon Telescope Collaboration], “First M87 Event Horizon Telescope Results. III. Data Processing and Calibration,” *Astrophys. J.* **875**, no. 1, L3 (2019) doi:10.3847/2041-8213/ab0c57 [arXiv:1906.11240 [astro-ph.GA]].
- [5] K. Akiyama *et al.* [Event Horizon Telescope Collaboration], “First M87 Event Horizon Telescope Results. IV. Imaging the Central Supermassive Black Hole,” *Astrophys. J.* **875**, no. 1, L4 (2019) doi:10.3847/2041-8213/ab0e85 [arXiv:1906.11241 [astro-ph.GA]].
- [6] K. Akiyama *et al.* [Event Horizon Telescope Collaboration], “First M87 Event Horizon Telescope Results. V. Physical Origin of the Asymmetric Ring,” *Astrophys. J.* **875**, no. 1, L5 (2019) doi:10.3847/2041-8213/ab0f43 [arXiv:1906.11242 [astro-ph.GA]].
- [7] K. Akiyama *et al.* [Event Horizon Telescope Collaboration], “First M87 Event Horizon Telescope Results. VI. The Shadow and Mass of the Central Black Hole,” *Astrophys. J.* **875**, no. 1, L6 (2019) doi:10.3847/2041-8213/ab1141 [arXiv:1906.11243 [astro-ph.GA]].
- [8] A. P. Porfyriadis, Y. Shi and A. Strominger, “Photon Emission Near Extreme Kerr Black Holes,” *Phys. Rev. D* **95**, no. 6, 064009 (2017) doi:10.1103/PhysRevD.95.064009 [arXiv:1607.06028 [gr-qc]].
- [9] J. M. Bardeen and G. T. Horowitz, “The Extreme Kerr throat geometry: A Vacuum analog of $AdS(2) \times S^{*2}$,” *Phys. Rev. D* **60**, 104030 (1999) doi:10.1103/PhysRevD.60.104030 [hep-th/9905099].
- [10] M. Guica, T. Hartman, W. Song and A. Strominger, “The Kerr/CFT Correspondence,” *Phys. Rev. D* **80**, 124008 (2009) doi:10.1103/PhysRevD.80.124008 [arXiv:0809.4266 [hep-th]].
- [11] M. Guo, P. C. Li and B. Chen, “Photon Emission Near Myers-Perry Black Holes in the Large Dimension Limit,” *Phys. Rev. D* **101**, no. 2, 024054 (2020) doi:10.1103/PhysRevD.101.024054 [arXiv:1911.08814 [gr-qc]].
- [12] S. E. Gralla, A. Lupsasca and A. Strominger, “Observational Signature of High Spin at the Event Horizon Telescope,” *Mon. Not. Roy. Astron. Soc.* **475**, no. 3, 3829 (2018) doi:10.1093/mnras/sty039 [arXiv:1710.11112 [astro-ph.HE]].

- [13] S. W. Wei, B. M. Gu, Y. Q. Wang and Y. X. Liu, “Photon emission of extremal Kerr–Newman black holes,” *Eur. Phys. J. C* **77**, no. 2, 128 (2017) doi:10.1140/epjc/s10052-017-4699-7 [arXiv:1608.04262 [gr-qc]].
- [14] A. Lupsasca, A. P. Porfyriadis and Y. Shi, “Critical Emission from a High-Spin Black Hole,” *Phys. Rev. D* **97**, no. 6, 064017 (2018) doi:10.1103/PhysRevD.97.064017 [arXiv:1712.10182 [gr-qc]].
- [15] M. Guo, N. A. Obers and H. Yan, “Observational signatures of near-extremal Kerr-like black holes in a modified gravity theory at the Event Horizon Telescope,” *Phys. Rev. D* **98**, no. 8, 084063 (2018) doi:10.1103/PhysRevD.98.084063 [arXiv:1806.05249 [gr-qc]].
- [16] D. Gates, D. Kapec, A. Lupsasca, Y. Shi and A. Strominger, “Polarization Whorls from M87 at the Event Horizon Telescope,” arXiv:1809.09092 [hep-th].
- [17] F. Long, S. Chen, J. Wang and J. Jing, “Electromagnetic emissions from near-horizon region of an extreme Kerr-Taub-Nut black hole,” *Eur. Phys. J. C* **79**, no. 6, 466 (2019) doi:10.1140/epjc/s10052-019-6989-8 [arXiv:1812.11463 [gr-qc]].
- [18] H. Yan, “Influence of a plasma on the observational signature of a high-spin Kerr black hole,” *Phys. Rev. D* **99**, no. 8, 084050 (2019) doi:10.1103/PhysRevD.99.084050 [arXiv:1903.04382 [gr-qc]].
- [19] T. Igata, H. Ishihara and Y. Yasunishi, “Observability of spherical photon orbits in near-extremal Kerr black holes,” *Phys. Rev. D* **100**, no. 4, 044058 (2019) doi:10.1103/PhysRevD.100.044058 [arXiv:1904.00271 [gr-qc]].
- [20] D. Kapec and A. Lupsasca, “Particle motion near high-spin black holes,” *Class. Quant. Grav.* **37**, no. 1, 015006 (2020) doi:10.1088/1361-6382/ab519e [arXiv:1905.11406 [hep-th]].
- [21] T. Igata, K. Nakashi and K. Ogasawara, “Observability of the innermost stable circular orbit in a near-extremal Kerr black hole,” arXiv:1910.12682 [astro-ph.HE].
- [22] M. Guo, S. Song and H. Yan, “Observational signature of a near-extremal Kerr-Sen black hole in the heterotic string theory,” *Phys. Rev. D* **101**, no. 2, 024055 (2020) doi:10.1103/PhysRevD.101.024055 [arXiv:1911.04796 [gr-qc]].
- [23] G. Compère and A. Druart, “Near-horizon geodesics of high-spin black holes,” *Phys. Rev. D* **101**, no. 8, 084042 (2020) doi:10.1103/PhysRevD.101.084042 [arXiv:2001.03478 [gr-qc]].
- [24] K. S. Thorne, “Disk accretion onto a black hole. 2. Evolution of the hole.,” *Astrophys. J.* **191**, 507 (1974). doi:10.1086/152991
- [25] F. Tamburini, B. Thidé and M. Della Valle, “Measurement of the spin of the M87 black hole from its observed twisted light,” *Mon. Not. Roy. Astron. Soc.* **492**, no. 1, L22 (2020) doi:10.1093/mnras/slz176 [arXiv:1904.07923 [astro-ph.HE]].

- [26] C. Bambi, K. Freese, S. Vagnozzi and L. Visinelli, “Testing the rotational nature of the super-massive object M87* from the circularity and size of its first image,” *Phys. Rev. D* **100**, no. 4, 044057 (2019) doi:10.1103/PhysRevD.100.044057 [arXiv:1904.12983 [gr-qc]].
- [27] S. Chandrasekhar, *The Mathematical Theory of Black Holes* (Oxford University Press, New York, 1983).
- [28] B. Carter, “Global structure of the Kerr family of gravitational fields,” *Phys. Rev.* **174**, 1559 (1968). doi:10.1103/PhysRev.174.1559